Hindawi
International Journal of Aerospace Engineering
Volume 2019, Article ID 6592972, 9 pages
https://doi.org/10.1155/2019/6592972

Research Article

Effects of Oxygen Content on the Ablation Behavior of Silicone Rubber-Based Insulation Material

Yi-ang Shi, Bai-lin Zha, Qing-dong Su, and Xu-dong Jia

206 Department, Rocket Force University of Engineering, Xi'an 710025, China

Correspondence should be addressed to Yi-ang Shi; shiyiang@gmail.com

Received 7 May 2019; Accepted 9 July 2019; Published 30 October 2019

Academic Editor: Rosario Pecora

Copyright © 2019 Yi-ang Shi et al. This is an open access article distributed under the Creative Commons Attribution License, which permits unrestricted use, distribution, and reproduction in any medium, provided the original work is properly cited.

A self-designed oxygen-kerosene ablation system was employed to research the ablation properties of silicone rubber-based insulation material under different oxygen-rich conditions, that is, 0%, 5.00%, 7.71%, 17.01%, and 18.50%. The morphology of posttest specimens was analyzed via a scanning electron microscope (SEM), and the ablation rates were calculated. Experimental results showed that when the particle concentration was a fixed value, the mass and the linear ablation rates increased first and then decreased with the rise of oxygen content; the maximum values were 0.572 g/s and 0.933 mm/s, respectively. Under high oxygen-rich conditions, the formation of silicone rubber restricted the further increase of the ablation rates, filling more gaps of the reaction layer with liquid silicone rubber. Meanwhile, the thickness of the liquid glass layer attached to the surface was increased, which acted as a buffer against the impacts and erosion of particles and retarded the consumption and recession of materials. Excess oxygen spread to the edge of the ablation pit and reacted. Finally, these led to the increase in diameter of the ablation pit and the decrease of two types of ablation rates.

1. Introduction

When a solid rocket ramjet (SRR) engine works, the heat protection component in the combustion chamber will suffer from the thermochemical ablation of oxygen-enriched gas, particle erosion of condensed matter, and aerodynamic erosion of high-speed gas, which brings higher requirements for the thermal protective performance of insulation materials. Because silicone rubber-based insulation material has a simple manufacturing process, low thermal conductivity, and a better resistance to oxygen-enriched eroding and superior smoke characteristic performance than ethylene propylene diene monomer (EPDM) insulation material, it is widely used as a thermal protection material of solid rocket ramjet combustor. In addition, when solid rocket ramjet engines operate at different altitudes, the oxygen-enriched environment will be changed accordingly, which will influence the ablation behavior of the thermal insulation layer. Therefore, it is of great practical significance to explore the influence of oxygen enrichment on the ablation behavior of the silicone rubber-based insulation material.

There have been many experiments testing the ablation properties of silicone rubber-based insulation materials. Baldwin from the US Navy Joint Institute developed a high-ethylene-component silicone rubber insulation coating, and the test results showed that the ablative performance of the new silicone rubber insulation coating was better than the general room temperature-vulcanized (RTV) silicone rubber [1]. The CELERG company put forward a variety of thermal insulation layer design schemes, and the feasibility of the schemes was verified by experiments [2]. Zhang et al. explored the impact factors of silicone rubber ablation performance according to formulas using different raw materials [3]. Wang et al. tested the influence of different gas environments on the ablation properties of silicone rubber insulation materials. Zhang et al. compared and analyzed the performance changes of the silicone rubber insulation material before and after engine tests [4]. Current research shows that researchers of ablation materials have paid more and more attention to silicone rubber-based insulation materials, and many research results have been obtained, which focused on material composition and formulation optimization.

Table 1: Formula of silicone rubber insulator.

Ingredients	Contents (phr*)
PDMS	50
PMPS	50
SiC	52
SiO_2	36
APP	10
Montmorillonite	5
Carbon fiber	5
Aramid fiber	1
ZrB_2	1

*Parts per hundred grams of rubber (phr).

However, limited by test methods, results of the influence of ablation atmosphere on the ablation behavior of silicone rubber-based insulation materials are scarce, and research on the ablation behavior of oxygen enrichment on silicone rubber-based insulation material is not found in the open literature.

In order to explore the influence of an oxygen-enriched environment on the ablation behavior of silicone rubber-based insulation material, this study sets the actual ablation of a solid rocket ramjet chamber insulation material as the research background, where a self-designed oxygen-kerosene simulation ablation test system was employed to conduct ablation experiments on the silicone rubber-based insulation material under different oxygen-rich conditions. This work analyzed the relationship between ablation rate and oxygen enrichment, focusing on the effect of oxygen enrichment on the ablation behavior of the silicone rubber-based insulation material by combining the macroscopic and microscopic ablation morphology and characteristics of the material.

2. Experimental

2.1. Materials. The raw materials included polydimethylsiloxane (PDMS), polydimethylphenylsiloxane (PMPS), SiC, fumed silica (silicon dioxide), ammonium polyphosphate (APP), montmorillonite, carbon fiber, aramid fiber, ZrB_2, and high silica fiber scrim, with the formula for the silicone rubber-based insulation material shown in Table 1.

After being weighed according to the formula, base rubber and various fillers were premixed and infiltrated for more than 4 hours, then dispersed via high-speed dispersion for half an hour. The mixture was stirred evenly and pressed into a piece by a mold after discharging air bubbles. Eventually, the surface of the piece of insulation material was covered with high silica fiber scrim before emerging as finished products [1].

In accordance with the actual experiential demand, the finished product was cut into a specimen with a size of $50 \times 50 \times 10$ mm (Figure 1), the density of which was about 1.61 g/cm^3.

2.2. Ablation Test System and Analytical Instruments. Aviation kerosene and oxygen served as fuel and combustion supporting agent, respectively, for the ablation test system, controlled by the operator console and stably transported to the ablation test motor. After atomization, the fuel mixed with oxygen in the combustion chamber to form a combustible mixed gas, then was ignited by a high-energy spark plug forming high temperature and high pressure gas, and was finally accelerated by a Laval nozzle to become a stable ablation gas jet. Meanwhile, the powders were injected via jet flow through a powder feeding port in the cavity wall of the ablation motor. After the powders were mixed, heated, and accelerated by gas, the specific gas-solid two-phase flow thermal environment that the experiment needs formed at the outlet of the nozzle. The ablation specimens were ablated by two-phase flow gas from the motor outlet. The particle concentration of two-phase flow could change (0%–30%), and the ablation angle was controllable (0°–90°), as seen in the schematic of the experiment system shown in Figure 2.

In the experiment, alumina powder, produced by sinter-crushing methods and with a particle size of 15–45 μm and purity higher than 99.4%, was injected into the jet. Figure 3

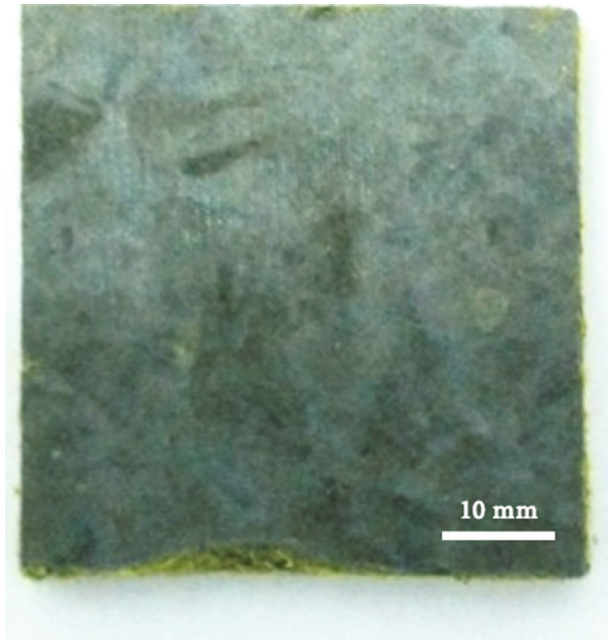

Figure 1: Morphology of the specimen before ablation.

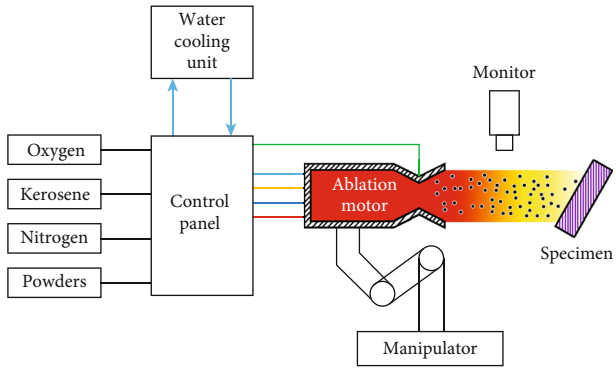

Figure 2: Schematic of the experiment system.

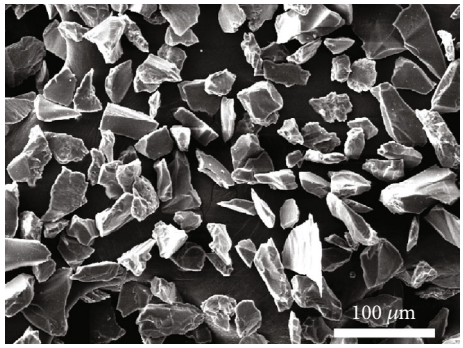

Figure 3: SEM photograph of the alumina powder.

Table 2: Parameters of the experiment system.

Item	Value
Ablation distance (mm)	80
Ablation angle (°)	45
Combustion chamber pressure (MPa)	0.27
Test time (s)	10

shows the micromorphology of the alumina powder, where it can be seen that the powder particles have an irregular shape and uniform size.

The analytical instruments used in the experiment include a VEGA II XMU scanning electron microscope (SEM) produced by the Czech TESCAN company and an Energy350 INCA energy spectrometer provided by the British OXFORD company.

2.3. Test Parameters. According to the characteristic parameters of the combustion chamber of a certain type of solid rocket ramjet engine, after the preliminary equivalence study, the initial oxygen flow rate of the ablation system was set to 338 L/min and the kerosene flow rate was 0.146 kg/min. Combustion chamber pressure was controlled at about 0.27 MPa. The ablation distance (the distance from the nozzle outlet to the surface of the specimen) was 80 mm according to the metal melting point method. The temperature of the jet touching the surface of the specimen was about 2000 K, and the speed was about 470 m/s by thermal calculation and simulation analysis, which could meet the practical requirements of the thermal insulation material ablation of the solid ramjet engine [5]. In the test experiment, because the ablation time was too long, the test specimen burned through, so the final ablation test time was set to 10 s. The specific parameter settings are shown in Table 2.

In order to ensure that the combustion chamber pressure was constant, the change of oxygen enrichment degree was achieved by adjusting the oxygen and kerosene flow rates to control the total mass flux invariant. The experiment included 5 designed groups of programs, each with 3 specimen pieces. The mean value of the ablation rate of 3 specimens was taken as the actual ablation rate of the group. The literature [6, 7] shows that the particles in the ablation jet have a great influence on the ablation behavior of materials, and previous research showed that the alumina particles have so high of a melting point that the gas cannot fully melt them, and the chilled, hard particles caused an erosion effect that had a great impact on the material. Thus, in order to avoid the effect of particle erosion on the degree of oxygen enrichment factors, the preliminary test results and the actual test parameters of a certain type of solid rocket ramjet engine were combined, and the experimental particle concentration was 0.24%. Specific test programs are shown in Table 3.

Table 3: Program of the ablation test.

Specimen group	Oxygen flux ($L \cdot min^{-1}$)	Kerosene flux ($kg \cdot min^{-1}$)	Oxygen-rich condition (%)	Particle concentration (%)
A	338	0.146	0	0.24
B	342	0.138	5.00	0.24
C	344	0.134	7.71	0.24
D	352	0.120	17.01	0.24
E	357	0.119	18.50	0.24

Table 4: Ablation rates of the specimens.

Specimen group	Mass ablation rate ($g \cdot s^{-1}$)	Mass ablation rate relative error (%)	Linear ablation rate ($mm \cdot s^{-1}$)	Linear ablation rate relative error (%)
A	0.477	5.17	0.800	3.78
B	0.487	3.37	0.871	2.44
C	0.506	1.77	0.933	3.65
D	0.572	5.76	0.865	2.61
E	0.568	3.64	0.852	5.13

3. Results and Discussion

3.1. Ablation Rate Measurement and Analysis. According to the calculation formula of mass ablation rate and linear ablation rate in literature [8], the ablation rates of the specimens are calculated and listed in Table 4, as visualized in Figure 4.

The data show that with the increase of oxygen enrichment, the two types of ablation rates are showing a trend of increasing first and then decreasing, the maximum linear ablation rate is 0.933 mm/s, the minimum line ablation rate is 0.800 mm/s, and the maximum value appears in the condition of 7.71% oxygen enrichment degree. The maximum mass ablation rate is 0.572 g/s, the minimum mass ablation rate is 0.477 g/s, and the maximum value appeared in the condition of 17.01% oxygen enrichment degree. The table shows that the ablation process of the silicone rubber-based insulation material has the ablation extreme value of oxygen enrichment degree.

3.2. Macroscopic Ablation Profile Analysis. The ablation morphologies of all specimens were basically similar, and the representative C2 was taken for macroscopic analysis. The appearance of the specimens is shown in Figure 5. The

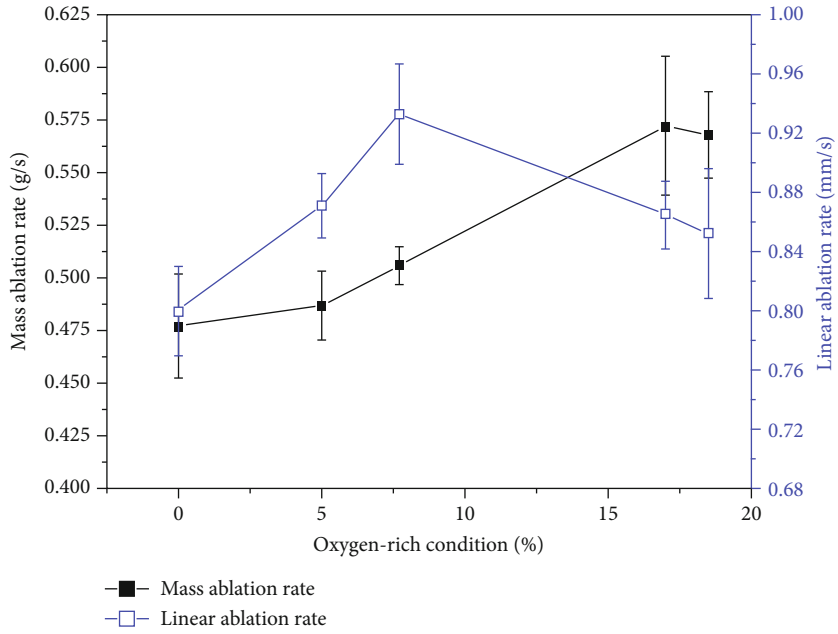

Figure 4: Ablation rate data diagram.

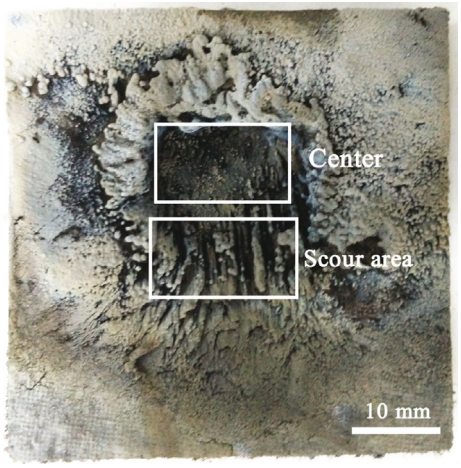

Figure 5: Ablation morphology of the specimen C2.

Figure 6: Section morphology of the specimen C2.

Table 5: Edge thickness of the reaction layer (mm).

Group	No. 1		No. 2		No. 3		Mean
	L	R	L	R	L	R	
A	0.99	1.13	1.03	1.10	1.11	1.05	1.07
B	1.09	1.07	1.12	1.06	1.01	1.09	1.07
C	1.18	1.23	1.32	1.26	1.19	1.29	1.25
D	1.29	1.27	1.35	1.44	1.37	1.41	1.36
E	1.45	1.53	1.39	1.42	1.40	1.48	1.45

overall ablation area was grayish white after the thermal decomposition of the material, and a large amount of molten material was separated out and blown from the specimen center to the edge of the ablation pit by high-speed flame flow. Then, this material accumulated to form a liquid-glass-layer-like molten residue. At the same time, due to erosion stripping of particles in the jet, there was bundle ablation gully morphology in the lower ablation pit of specimens along the 45-degree direction that was the ablation angle. With the increase of oxygen enrichment degree, the ablation pit size of the specimen increased gradually.

Specimen C2 was cut transversely, and ablation stratification was observed as shown in Figure 6. The naked eye can directly see the interface between the reaction layer and the virgin layer, but the ceramic layer and the pyrolytic layer in the reaction layer were not easy to distinguish. The figure also shows that the pyrolytic layer and the ceramic layer have continuity and similarity in morphology.

According to the temperature distribution of the plume, it can be inferred that the thickness of the ceramic layer covered on the silicone rubber surface should appear from the center to the edge as a gradually thinning phenomenon. However, with a flame center jet speed and chilled particle concentration, the damage is also the strongest, and the erosion effect of the central area is far stronger than that of the edge area. With the continuous erosion of the flame current, the ceramic layer in the central area is destroyed, leaving only the thin ceramic layer attached to the surface of the specimen. As a result of this phenomenon, the ceramic layer in the ablation center is thinner, and in the area outside the ablation pit, the farther away from the pit, the thinner the ceramic layer is [9].

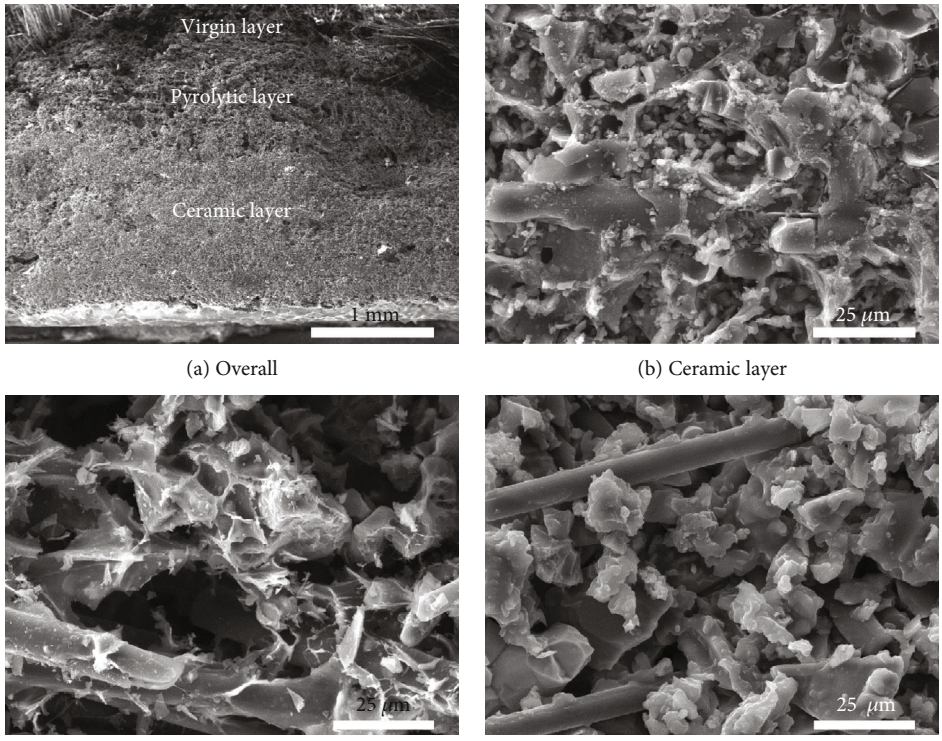

(a) Overall (b) Ceramic layer

(c) Pyrolytic layer (d) Virgin layer

Figure 7: Section morphology of the specimen E3 at different positions.

After each specimen was cut transversely, the thickness of the reaction layer on the left and right sides in the section of each specimen was measured, shown in Table 5 (L represents the left edge, R represents the right edge). The average thickness of the reaction layer increased as the oxygen enrichment degree increased slightly because the oxidizing component driven by oxygen concentration penetrated deeper. Thus, in accordance with the pyrolytic reaction process, the surface reaction layer thickness was increased [10].

3.3. Microscopic Ablation Profile Analysis. A section of specimen E3 was magnified to obtain the layered morphology, as shown in Figure 7(a). After further magnification, the microstructures of the ceramic layer, the pyrolytic layer, and the virgin layer are shown in Figures 7(b)–7(d), respectively. Among these, the ceramic layer was compact. The pyrolytic layer had many gas holes and a loose structure [11], and a large amount of pyrolysis gas was produced during the severe oxidation pyrolysis reaction, leading to the formation of a large number of pore gaps after the pyrolysis. The virgin layer consisted of different sizes and shapes of reinforcing filler composition. According to the energy spectrum analysis results, the content of elemental Si was the highest in the matrix material, and the flow attachment on material surface was SiO_2, which was from the spillover of the silicon group in the reaction layer after oxidation and melting [12].

Bundle structures were observed in all the gully scour area of specimens. Under different oxygen-rich conditions, the micro morphological characteristics of the scour area were slightly different. From Figures 8(a) and 8(b), it can be seen that under high oxygen-rich conditions, the bundle structure size decreased, and meanwhile, the bundle and pore structure on the surface of gully scour area increased significantly. A gap between the bundle structures was formed by the high-speed particle erosion. After increasing the magnification to 500, bundle structures were observed, as shown in Figures 8(c) and 8(d), and it was found that a large number of floc attached to the bundle structures' surface. The elemental analysis results of the scour area are shown in Table 6, which indicated that the floc was mainly silicon dioxide. A large amount of silicon dioxide in pyrolysis products and fillers were attached to the bundle structures' surface after melting precipitation. Comparing the composition of the elements in the erosion area under different oxygen enrichment conditions, it could be determined that the content of elemental carbon clearly decreased when the oxygen enrichment increased, indicating the formation of floc structure material directly related to oxygen enrichment conditions [13, 14].

The ablation process was a process of oxidation of carbon and silicon. Gaseous products such as carbon dioxide in the oxidation products were removed by high-speed gas flow. The silicon dioxide and other materials, which were in the molten state, were precipitated from the interior and attached to the surface of the material and then blown away by the flame flow shearing force. Under the conditions of high oxygen enrichment, the precipitation of silicon dioxide was greater, resulting in the decrease of carbon element content and the rise of silicon element content.

Figure 9 shows the ceramic layer microscopic morphology in the center of the specimens under different oxygen-rich

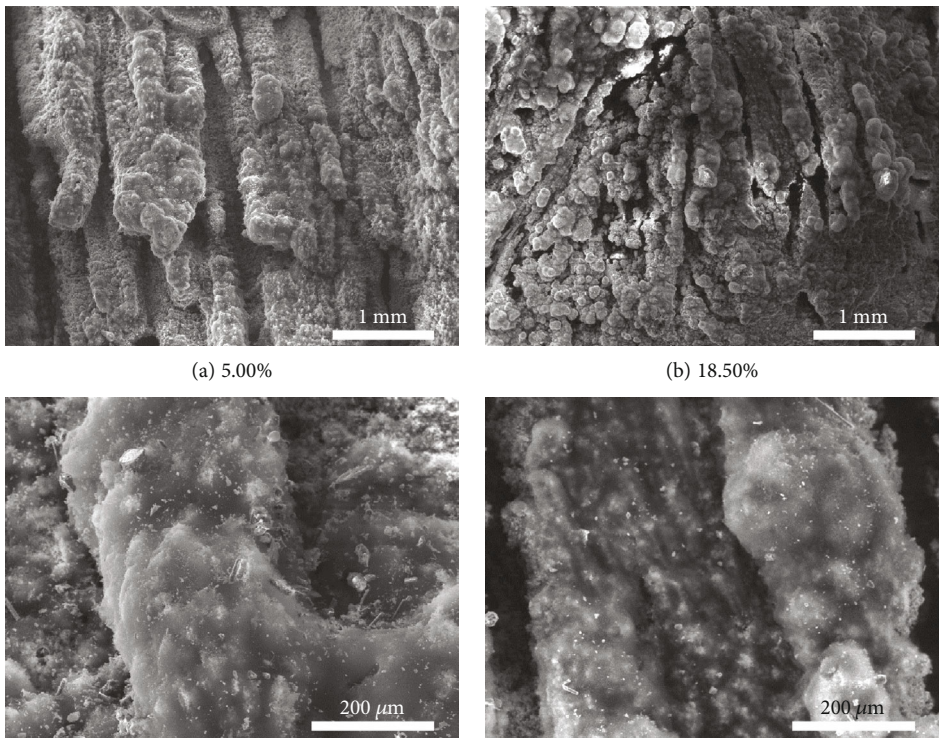

(a) 5.00% (b) 18.50%

(c) 5.00% (d) 18.50%

Figure 8: Ceramic layer morphology in the scour area under different oxygen-rich conditions.

Table 6: Atomic percentage of the scour area under different oxygen-rich conditions.

Element	Before ablation	Oxygen-rich 5.00%	Oxygen-rich 18.50%
C	22.52	10.44	4.5
O	38.73	62.04	67.27
Si	38.75	27.52	28.22

conditions. Table 7 shows the result of the surface scanning element analysis in the corresponding domain. There were compact structures on the ceramic layer surface of various specimens combined with granular materials of different sizes, which served as a good protection for the ceramic layer below the structure and ensured that the insulation material had good resistance to erosion and ablation.

When the surface of the material was heated, the ceramic layer was formed by pyrolysis, and the main chemical reactions in the process included the decomposition of the rubber matrix and the oxidation of the decomposition products and the filler. A large number of Si-O and Si-C chains had been separated from the side chain scission of PDMS and PMPS, which would be further oxidized to silicon dioxide; at the same time, the silicon carbide filler reacted with the oxidizing component to produce silicone rubber and carbon dioxide, in which carbon dioxide was released from the ceramic layer gap and was taken away by the flame [15]. However, with the impact of flame heating, the surface temperature continues to rise; when the temperature rose to a critical temperature, a great quantity of silicone rubber separated out from the gap of the ceramic layer gradually after melting. Driven by the adhesive force, liquid silicone rubber had an accumulation effect on the surface, and the liquid glass layer played a buffering role in the impact erosion of particles; meanwhile, the reverse migration process blocked the positive transfer of some heat [5, 9].

When the oxygen enrichment degree was less than the extreme point, increasing oxygen enrichment would promote the pyrolysis oxidation reaction of the materials and speed up the consumption of material in the center; when the oxygen enrichment degree was increased to more than the extreme point, the formation of silicone rubber would be the main factor to restrict the ablation rate [9]. According to the porosity results in Figure 10 (obtained by Morpholog, the image processing module of the SEM, adopting a watershed algorithm to process image gray value for judging boundary), under high oxygen enrichment conditions, more of the gap in the reaction layer was filled with liquid silicon dioxide [16]; at the same time, because of the strong adhesive force, the thickness of the liquid glass layer attached to the surface rose, which would play a better role in buffering the particles and slow down the consumption and the movement of the material.

However, the excess oxygen would diffuse to the edge of the ablation pits and react with the edge materials, which would eventually result in the increase of the diameter of the ablation pits and the decrease of the two types of ablation rates.

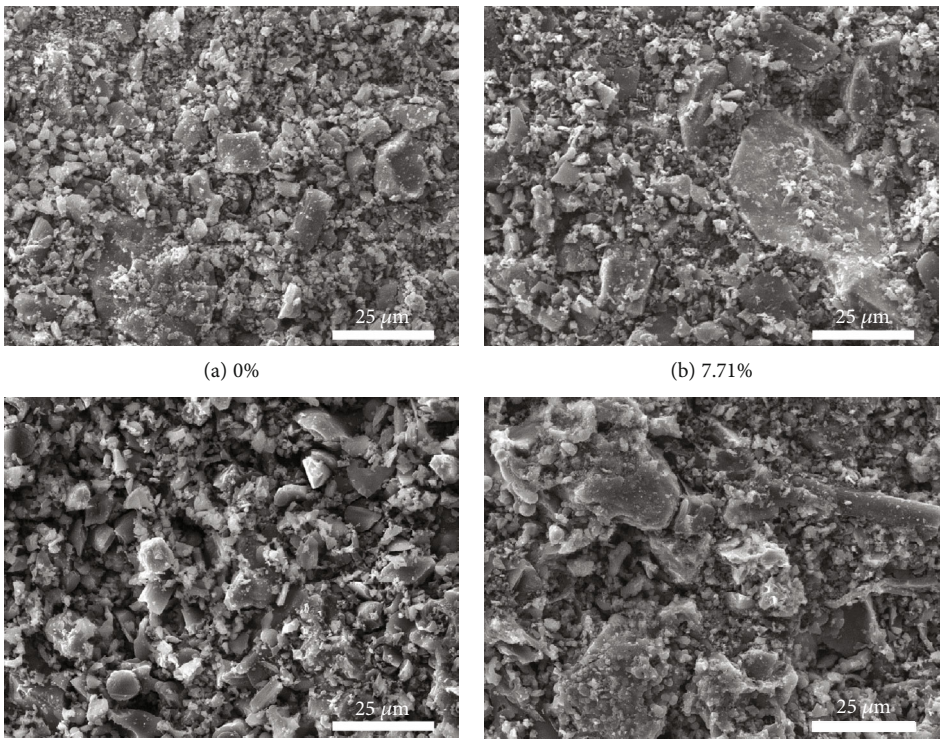

(a) 0% (b) 7.71%

(c) 17.01% (d) 18.50%

Figure 9: Ceramic layer morphology in the center under different oxygen-rich conditions.

Table 7: Atomic percentage of the ceramic layer in the center under different oxygen-rich conditions.

Element	Oxygen-rich 0	Oxygen-rich 7.71%	Oxygen-rich 17.01%	Oxygen-rich 18.50%
C	22.41	24.61	26.32	19.6
O	44.66	45.31	45.16	48.53
Si	32.93	30.08	28.52	31.87

4. Conclusion

(1) The mass ablation rate and linear ablation rate of the material showed a trend of first increasing and then decreasing with the increase of oxygen enrichment degree. When the particle concentration was 0.24%, the maximum linear ablation rate was 0.933 mm/s, which occurred under the condition of 7.71% oxygen enrichment degree, and the maximum mass ablation rate was 0.572 g/s, where the corresponding oxygen enrichment degree was 17.01%

(2) There were bundle structures in the gully scour area of the specimens, and the floc attached to the surface of bundle structures was silicone rubber. With the increase of the oxygen enrichment degree, the oxidation and ablation effect of the oxidative component to the gully structure between the bundle increased, the bundle structure became finer, more pores on the surface of gully scour area appeared, and the carbon element content decreased

(3) When the oxygen enrichment degree was less than the extreme point, increasing oxygen enrichment would promote the pyrolysis oxidation reaction of materials and speed up the consumption of material in the center. When the oxygen enrichment degree was increased to more than the extreme point, the formation of silicone rubber would be the main factor to restrict the ablation rate. Under high oxygen enrichment conditions, more of the gap in the reaction layer was filled with liquid silicon dioxide; at the same time, because of the strong adhesive force, the thickness of the liquid glass layer attached to the surface rose, which would play a better role in buffering the particles and slowing down the consumption and the movement of the material. However, the excess oxygen would diffuse to the edge of the ablation pits, which would eventually result in the increase of the diameter of the ablation pits and the decrease of the two types of ablation rates

(4) Engineers can locate the oxygen enrichment extreme value point of extreme ablation according to the experiment results. On this basis, the ablation rates obtained can be used to evaluate insulation performance in order to optimize the local thickness for minimizing negative structural quality. In addition, the afterburner structure of SRR, such as intake form and air-inlet area, can be better designed to adapt to the optimum flow ratio

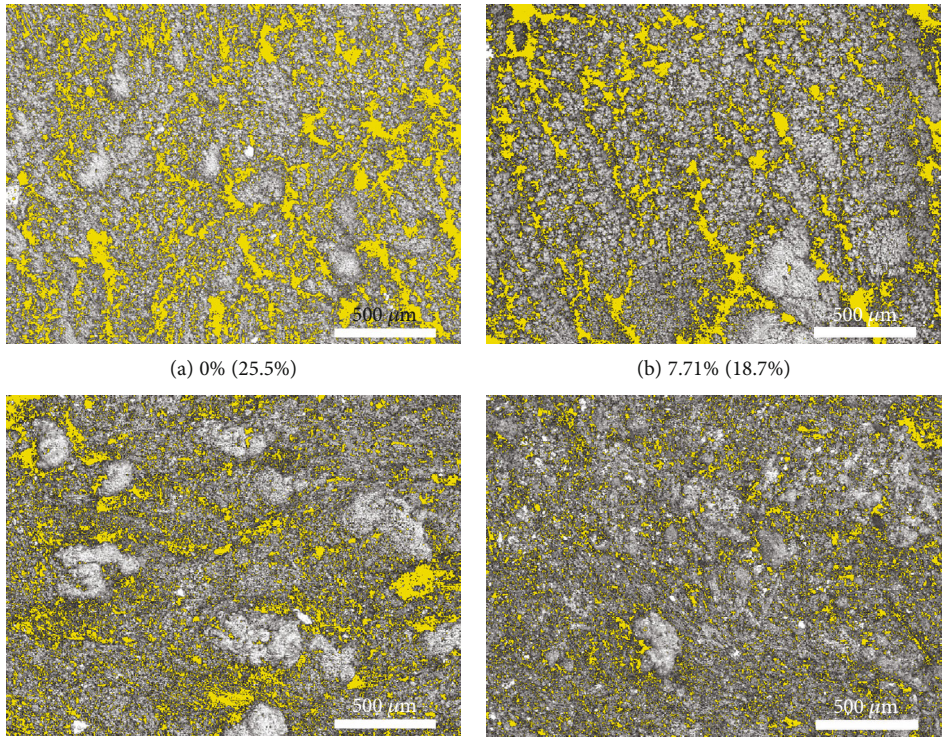

(a) 0% (25.5%) (b) 7.71% (18.7%)

(c) 17.01% (17.4%) (d) 18.50% (11.4%)

Figure 10: Porosity ratio image of the ceramic layer under different oxygen-rich conditions.

This method is an effective technical approach for performance evaluation and mechanism analysis under various ablation test conditions matching the larger flight region of the SRR.

Data Availability

The data used to support the findings of this study are included within the article.

Conflicts of Interest

The authors declare that they have no conflicts of interest.

References

[1] Y. Zhang, G.-h. Chen, and J.-g. Wang, "Study on thermal protection of silicon rubber insulation used in the ramjet afterburner," *Chinese Journal of Explosives and Propellants*, vol. 30, no. 3, pp. 65–68, 2007.

[2] S. Yamada and C. Serizawa, *Thermal and Ablative Properties of Silicone Insulation, AIAA 97-3259*, AIAA, New York, NY, USA, 1997.

[3] C.-G. Zhang, G.-L. Lu, J.-S. Zhang, and Y.-L. Zhu, "Ablative properties of silicone rubber heat shields," *Silicone Material*, vol. 19, no. 1, pp. 1–4, 2005.

[4] Y. Zhang, H.-m. Shu, and Y.-j. Shi, "Analysis on performance change of silicone rubber insulation layer in solid ramjet motor after test," *Chemical Propellants & Polymeric Materials*, vol. 12, no. 1, pp. 49–56, 2014.

[5] L. Li, T. Yang, X.-h. Cheng, and L. Yang, "Ablation model of silicon insulator in ramjet combustion chamber," *Journal of Propulsion Technology*, vol. 33, no. 3, pp. 451–454, 2012.

[6] C. T. Crowe, T. R. Troutt, and J. N. Chung, "Numerical models for two-phase turbulent flows," *Annual Review of Fluid Mechanics*, vol. 28, no. 1, pp. 11–43, 1996.

[7] L. Li, T. Yang, and W. Jiang, "Effcets of high-velocity particles on solid ramjet insulator," *Journal of Projectiles Rockets Missiles and Guidance*, vol. 32, no. 1, pp. 127–130, 2012.

[8] *GJB 323A-96 Test Methods for Ablation of Ablators*, 1996.

[9] D. Yang, *Silicone Rubber Based Insulation Material and Its Thermochemical Ablation Mechanism*, National University of Defense Technology, Changsha, China, 2013.

[10] Y.-K. Chen, *Thermal Ablation Modeling for Silicate Materials, AIAA 2016-1514*, AIAA, San Diego, CA, USA, 2016.

[11] D. Yang, W. Zhang, and B.-z. Jiang, "Ceramization and oxidation behaviors of silicone rubber ablative composite under oxyacetylene flame," *Ceramics International*, vol. 39, no. 2, pp. 1575–1581, 2013.

[12] C. Chunjuan and M. Guofu, "Study on internal insulation of rocket engine in oxidizer rich environment," *Journal of Rocket Propulsion*, vol. 30, no. 4, pp. 32–35, 2004.

[13] C. Zhou, L. Yu, W. Luo, Y. Chen, H. Zou, and M. Liang, "Ablation properties of aluminum silicate ceramic fibers and calcium carbonate filled silicone rubber composites," *Journal of Applied Polymer Science*, vol. 132, no. 11, 2015.

[14] V. V. Nesmelov, V. D. Gol'din, and G. F. Kostin, "Ablation characteristics of thermal protective materials based on carbon

fiber reinforced composites," *Combustion, Explosion and Shock Waves*, vol. 39, no. 3, pp. 309–315, 2003.

[15] E. S. Kim, E. J. Kim, J. H. Shim, and J.-S. Yoon, "Thermal stability and ablation properties of silicone rubber composites," *Journal of Applied Polymer Science*, vol. 110, no. 2, pp. 1263–1270, 2008.

[16] S.-x. Wang and J. Li, "Experimental analysis of silicon rubber insulator thermo-chemical ablation characteristics," *Science Technology and Engineering*, vol. 15, no. 15, pp. 218–221, 2015.

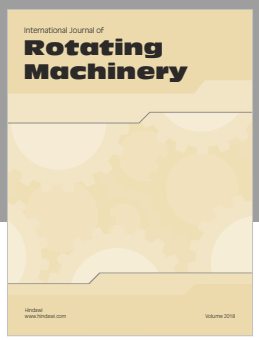

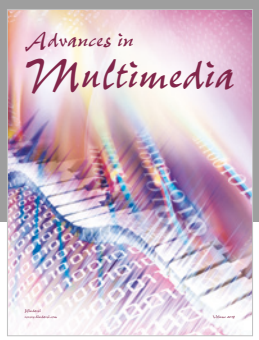

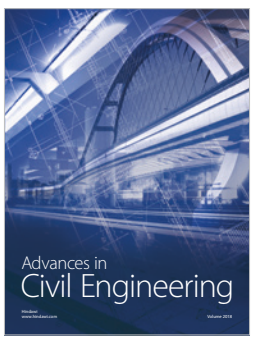

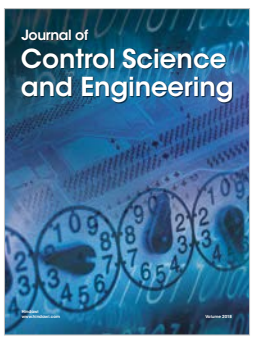

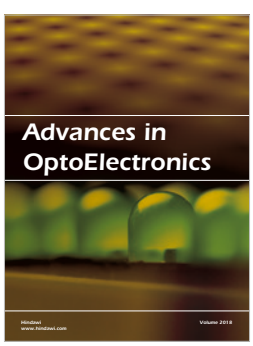

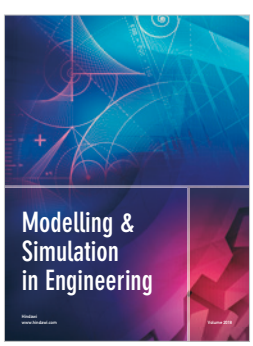

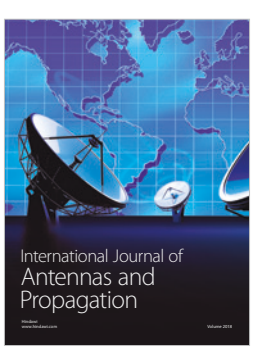

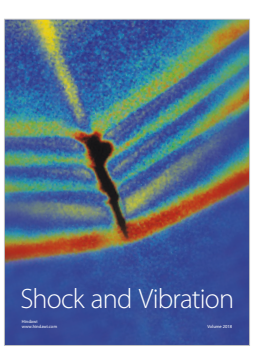

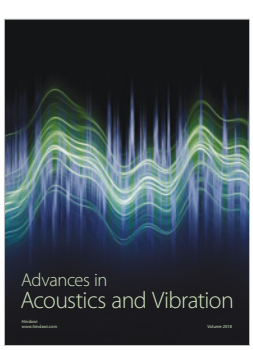

Hindawi

Submit your manuscripts at
www.hindawi.com